Journal of Catalysis 304 (2013) 123–134

Contents lists available at SciVerse ScienceDirect

Journal of Catalysis

journal homepage: www.elsevier.com/locate/jcat

Conversion of glucose into levulinic acid with solid metal(IV) phosphate catalysts

Ronen Weingarten [a], Yong Tae Kim [a], Geoffrey A. Tompsett [b], Alejandro Fernández [b], Kee Sung Han [c], Edward W. Hagaman [c], Wm. Curt Conner Jr. [b], James A. Dumesic [a], George W. Huber [a,*]

[a] Univeirsty of Wisconsin–Madison, Department of Chemical and Biological Engineering, 1415 Engineering Dr., Madison, WI 53706, USA
[b] University of Massachusetts–Amherst, Department of Chemical Engineering, 159 Goessmann Lab, 686 North Pleasant St., Amherst, MA 01003, USA
[c] Oak Ridge National Laboratory, Chemical Sciences Division, Building 4100, Room A123, 1 Bethel Valley Rd., Oak Ridge, TN 37831, USA

ARTICLE INFO

Article history:
Received 27 September 2012
Revised 22 January 2013
Accepted 26 March 2013
Available online 25 May 2013

Keywords:
Metal(IV) phosphate
Solid acid catalyst
Glucose
Levulinic acid
Brønsted
Lewis
Dehydration
Aqueous phase

ABSTRACT

We have prepared a series of well-characterized solid acid metal(IV) phosphate catalysts and tested them for the two-step dehydration/rehydration reaction to produce levulinic acid from glucose. The catalysts include zirconium (ZrP) and tin (SnP) phosphates with varying ratios of phosphorus to metal(IV). The structural, surface and bulk properties have been investigated using XRD, BET, XPS and ^{31}P solid-state MAS NMR spectroscopy. ZrP is distinguished by a high concentration of polyphosphate species in the bulk phase, as well as increased hydroxyl groups on the surface. ZrP also shows a higher concentration of total acid sites and Brønsted acid sites compared to SnP, as determined by TPD measurements using gas-phase NH_3 and isopropylamine. The catalyst selectivity is a function of the Brønsted to Lewis acid site ratio using either heterogeneous or homogeneous catalysts. Catalytic activity increases with increased Lewis acid sites. The Lewis sites mainly produce fructose *via* isomerization reactions and undesired degradation products (humins). HMF is produced on both Brønsted and Lewis sites, whereas levulinic acid is exclusively produced on Brønsted sites. Zirconium phosphate with a P/Zr molar ratio of 2 is favorable for levulinic acid production due to its inherently high surface area and enhanced Brønsted acidity. This study lays the grounds for further design of improved solid acid catalysts for aqueous phase production of HMF and levulinic from carbohydrates.

1. Introduction

Decline of petroleum supplies and increased levels of greenhouse gases in the atmosphere have stimulated a worldwide initiative to develop clean technologies that utilize a sustainably produced feedstock. Lignocellulosic biomass is a renewable feedstock that has received considerable attention as a sustainable alternative for the production of fuels and chemicals [1–10]. In contrast to other renewable energies, biomass is the only renewable source of fixed carbon, which is essential for the production of liquid hydrocarbon fuels and chemicals [11–13]. One of the key sugar-based building blocks that can be obtained from lignocellulosic biomass is levulinic acid, which has been identified by the US Department of Energy as a top platform chemical [14,15]. Levulinic acid is a five carbon molecule with carboxylic acid and ketone functionalities, and the existence of these two functional groups provides this compound with interesting reactivity pathways.

As a top platform chemical, levulinic acid is the building block to produce a great number of bio-chemicals such as succinic acid, resins, polymers, herbicides, pharmaceuticals, flavoring agents, solvents, plasticizers, and anti-freeze agents. In particular, some levulinic acid derivatives can be used for fuels and oxygenated fuel additives. Esterification of levulinic acid with C_1–C_2 alcohols produces levulinic esters which can be used as diesel additives [16]. Elliott and Frye have also shown that levulinic acid can be hydrogenated in the presence of a bifunctional catalyst to produce methyl-tetrahydrofuran (MTHF) [17], which can directly serve as a gasoline blendstock [18]. Levulinic acid can also undergo hydrogenation to produce γ-valerolactone (GVL) [19–21], which has been shown to be a sustainable liquid transportation fuel suitable of replacing ethanol in gasoline–ethanol blends [22]. Lange et al. have shown that continued hydrogenation of GVL produces valeric acid which can be esterified with alcohols to produce a new class of cellulosic transportation fuels, "valeric biofuels" [23]. Bond et al. developed an integrated catalytic process to convert GVL to liquid alkenes (ranging from C_8 to C_{24}) which could be blended with gasoline, diesel or jet fuels [24].

* Corresponding author. Address: 4631 Engineering Hall, 1415 Engineering Dr., Madison, WI 53706, USA. Fax: +1 608 262 5434.
E-mail addresses: rweingarten@wisc.edu (R. Weingarten), exkimyt@gmail.com (Y.T. Kim), tompsett@ecs.umass.edu (G.A. Tompsett), jandro.fs@hotmail.com (A. Fernández), hanks@ornl.gov (K.S. Han), hagamanew@ornl.gov (E.W. Hagaman), wconner@ecs.umass.edu (W.C. Conner Jr.), dumesic@engr.wisc.edu (J.A. Dumesic), huber@engr.wisc.edu (G.W. Huber).

0021-9517/$ - see front matter © 2013 Elsevier Inc. All rights reserved.
http://dx.doi.org/10.1016/j.jcat.2013.03.023

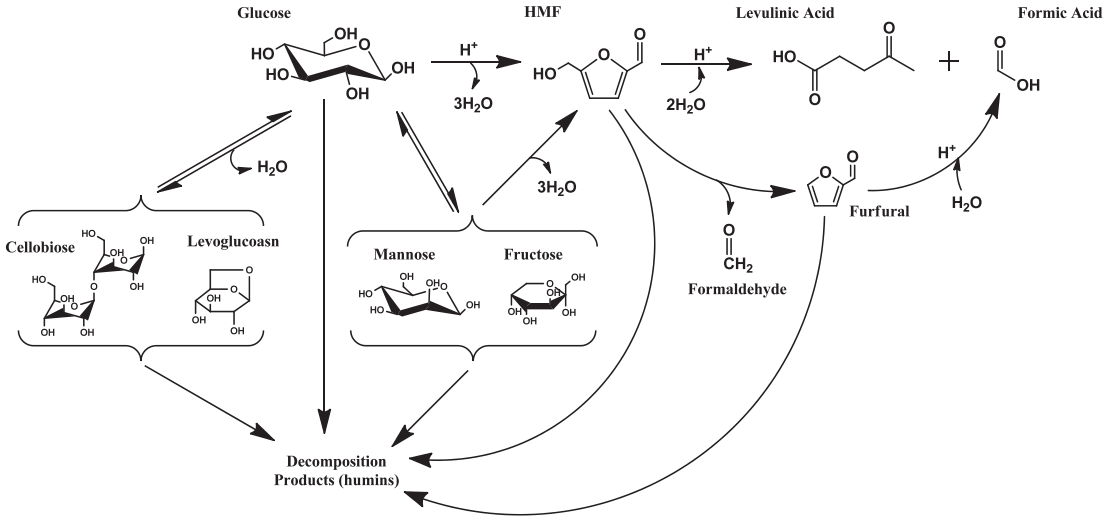

Fig. 1. Reaction pathway scheme for the conversion of glucose to levulinic acid.

Levulinic acid is produced through acid-catalyzed dehydration of hexose sugars. Among these, glucose is the most abundant in nature, available in the polysaccharide form as starch or cellulose in biomass [25]. Levulinic acid is produced from glucose by way of a two-step acid-catalyzed reaction (Fig. 1). We have studied the kinetics of levulinic acid production from aqueous glucose solutions with a homogeneous acid catalyst in a continuous regime [26]. Overall, there are four parallel pathways in which glucose can react: (1) Reversion reactions can lead to the formation of cellobiose and levoglucosan [27–29]; (2) degradation reactions to form highly polymerized carbonaceous species (i.e. humins); (3) epimerization reactions to form fructose and mannose [28], and (4) dehydration to produce 5-hydroxymethylfurfural (HMF). It has been reported that reversion and epimerization products can also decompose to form humins [30]. The humins are both water soluble and water insoluble. Water-soluble humins polymerize with time to form water-insoluble compounds. The isomerization of glucose into fructose has been reported to be favored by the presence of Lewis acid sites [31–33]. Recent studies have reported the efficient conversion of glucose to HMF using a combination of Lewis and Brønsted acid catalysts in a biphasic reactor system with 2-s-butylphenol as the extracting solvent [34,35]. The reaction proceeds through a tandem pathway including isomerization of glucose to fructose followed by dehydration of fructose to HMF. Subsequently, HMF can rehydrate to produce levulinic acid and formic acid. HMF can also decompose to produce humins and produce furfural *via* loss of formaldehyde [36–39]. Furfural can also undergo degradation reactions to form humins [40]. Formic acid is also a by-product of furfural degradation by way of hydrolytic fission of the furfural aldehyde group [41,42].

Attempts have been made to utilize recyclable solid acid catalysts to produce levulinic acid from biomass feedstocks. These range from zeolites and novel metal oxides to acidic ion-exchange polymer resins [43]. In particular, metal(IV) phosphate catalysts have shown to be selective and active for aqueous phase acid-catalyzed dehydration and isomerization reactions [44–47]. Extensive investigations have been carried out to determine the physicochemical and acidic properties of these catalysts [48,49]. Studies have shown that the amorphous form of these catalysts demonstrate higher activity due to increased overall acidity and surface area compared to their crystalline analog [50,51]. In addition, metal(IV) phosphates are beneficial as catalyst supports for metal oxides due to their textural and acid properties [52–54].

In the field of biomass conversion, various studies have been reported on the selective production of HMF from carbohydrates in the aqueous phase using metal phosphates as solid acid catalysts [55–58]. More recently, we found that amorphous zirconium phosphate containing a high Brønsted to Lewis acid site ratio exhibits high selectivity for furfural production from xylose [40]. The activity and selectivity for furfural production of the zirconium phosphate were comparable to those obtained from dehydration reactions with HCl. The dehydration of sorbitol to produce isosorbide with metal(IV) phosphates has also been reported [59]. Li et al. have found that platinum supported on zirconium phosphate serves as a stable, selective, and active catalyst for aqueous phase hydrodeoxygenation of aqueous sugar solutions to produce high-octane gasoline [60,61]. They found the catalyst to be stable in aqueous media at high temperatures (245 °C), and no deactivation occurred after 200 h time-on-stream. ICP studies confirmed that no leaching occurred. This coincides with a study by Asghari et al. who also found zirconium phosphate to be stable under subcritical water conditions [62]. Niobium-based catalysts have also received much consideration as solid acid catalysts due to their hydrothermal stability and high activity for aqueous phase dehydration of alcohols to olefins [63,64].

Zirconium phosphate has unique properties as a solid acid catalyst in that it is compatible in aqueous media. Various studies have investigated the source of the active sites on this class of catalysts. In their study of crystalline zirconium phosphate, Hattori et al. concluded that the catalyst possesses weak and strong acid sites, both of which are derived from P(OH) groups [65]. Clearfield and Thakur observed a decrease in the activity of zirconium phosphate after poisoning the catalyst with quinoline or following proton exchange with Cs^+ on the catalyst surface [44,48]. They correlated the active sites to surface hydroxyl groups but also associated some of the activity to Lewis-type sites. La Ginestra et al. used a similar surface poisoning technique to conclude that the catalytic activity of zirconium phosphate was solely from Brønsted acid sites on the surface of the catalyst [45]. Sinhamahapatra et al. observed both Brønsted and Lewis acid sites in their study on mesoporous zirconium phosphate [66]. They postulated that the Brønsted acid sites possibly arise from geminal P(OH) groups. The Lewis acid centers could be attributed to Zr^{4+}, as suggested by Spielbauer et al. [67].

The objective of this study is to characterize the different catalytic sites on supported metal(IV) phosphate solid acid catalysts and identify their roles in catalyzing the aqueous phase conversion

of glucose to produce levulinic acid. The nature of the metal(IV) and phosphorus loading will be investigated, as well as the role of Lewis and Brønsted acid sites. Common gas-phase characterization techniques will be used to determine the concentration and type of the acid sites, including temperature-programmed desorption using ammonia and isopropylamine as probe molecules. Additional techniques such as XPS, ICP, and ^{31}P solid-state NMR will be employed to study the surface and bulk properties of the solid acid catalysts.

2. Experimental

2.1. Catalyst preparation

The zirconium phosphate catalysts (ZrP) were prepared following procedures previously reported [51], which consisted of precipitation of $ZrCl_2O{\cdot}8H_2O$ (Sigma Aldrich, 1 mol L^{-1}, 140 mL) and $NH_4H_2PO_4$ (Sigma Aldrich, 1 mol L^{-1}, 280 mL) at a molar ratio of P/Zr = 2 (ZrP2). The solution was stirred at room temperature and then filtered, washed with de-ionized (DI) water until pH 5 and dried overnight at 373 K. The catalyst was powdered and calcined at 673 K for 4 h in air prior to reaction. The other two zirconium phosphate catalysts (ZrP1 and ZrP3) were prepared following the same procedure but varying the molar ratio of P/Zr to 1 and 3 respectively.

The tin phosphate catalyst (SnP1) was obtained following a procedure reported by Patel et al. [47]. A 0.1 M aqueous solution of disodium hydrogen phosphate (Sigma Aldrich, ReagentPlus™ ⩾99%) was added drop wise to an equimolar, equivolume, stirred aqueous solution of tin tetrachloride ($SnCl_4{\cdot}5H_2O$, Fisher Scientific). The resulting gel was stirred at 50 °C for 2 h and at room temperature for 24 h. It was then filtered and dried at room temperature. The dried material was powdered and converted to the hydrogen form by treatment with a 1 M aqueous solution of HNO_3 (Fisher Scientific) for 3 h, the acid being intermittently replaced with a fresh batch. It was then washed several times with de-ionized water to remove the excess acid until pH of 3 and finally dried at room temperature. Tin phosphate (SnP2) was prepared following the same procedure but varying the molar ratio of P/Sn to 2 and then washed thoroughly until pH 3.

Zirconium oxide was obtained by calcining zirconium hydroxide (supplied by MEL chemicals-(XZO 880/01)) at 673 K for 2 h in air. Hydrochloric acid was supplied by Fischer Scientific. Ytterbium (III) trifluoromethanesulfonate hydrate, Yb $(OTf)_3$, was supplied by Strem Chemicals.

2.2. Catalyst characterization

Total acid sites were determined by temperature-programmed desorption of ammonia (NH_3-TPD) with a Quantachrome ChemBET Pulsar™ TPR/TPD Automatic Chemisorption Analyzer coupled with a thermal conductivity detector (TCD) to quantify the ammonia desorbed from the sample. A sample of approximately 300 mg was initially degassed at 673 K for 1.5 h under a constant helium flow of 12 mL min^{-1} (Airgas, UHP). The sample was cooled and ammonia (Airgas, electronic grade) was adsorbed at 373 K for 30 min to reach saturation. Afterward, the ammonia supply line was shut off and helium was purged at 12 mL min^{-1} for 2 h to remove any physically adsorbed ammonia. The sample was then heated linearly at a rate of 10 K min^{-1} from 373 to 973 K (773 K for the tin phosphate samples) under a constant helium flow of 12 mL min^{-1}. The sample was held at the temperature set point for an additional 2 h.

The concentration of Brønsted acid sites was determined by temperature-programmed desorption of isopropylamine (IPA-TPD) with thermogravimetric analysis–mass spectrometry (TA instruments SDT Q600 system), as reported by Gorte et al. [68–70] Approximately 50–60 mg of sample was loaded and degassed at 673 K for 1.5 h under a constant helium flow of 100 mL min^{-1} (Airgas, UHP). The sample was then cooled to 318 K, at which point isopropylamine was bubbled with helium and adsorbed for 15–20 min. After saturation, the isopropylamine supply line was shut off and helium was purged at 100 mL min^{-1} to remove any physically adsorbed isopropylamine. The sample was then heated linearly at a rate of 10 K min^{-1} from 318 to 973 K (773 K for the tin phosphate samples) under a constant helium flow of 100 mL min^{-1}. During the TPD analysis, the signal m/z 39 (propylene) was monitored by the mass spectrometer. The mass spectrometer was calibrated for propylene (Sigma Aldrich, ⩾99%) for quantification purposes.

Adsorption and desorption isotherms (40 points each) of nitrogen were obtained for all of the samples at 77 K using a Quantachrome Autosorb® iQ2 automated gas sorption system. The surface areas were calculated using BET analysis ranging from 0.05 to 0.3 relative pressure P/P_o on the adsorption branch, and the BET "C" constants were recorded. The samples were degassed before each experiment at 523 K for 12 h.

XPS measurements were performed using a Physical Electronics Quantum 2000 Scanning ESCA Microprobe equipped with a monochromatic Al Kα anode (1486.6 eV). Samples were prepared by dusting them on double sided adhesive tape. They were then evacuated and placed on the stage of the instrument. Charging was neutralized using the turnkey electron/ion system, so that the C1s peak was fixed at 284.0 eV. Analysis was performed by taking sequential spectra from a 5° take-off angle increasing the angle by 3° per spectrum until the C1s line increased. Since this indicated that the substrate tape was detected, the angle was then decreased to that before the tape was detected. This proved to be a 15° take-off angle which provided excellent signal to noise for quality spectra, acquired using a 200 μm spot at 50 W. All quantitative calculations used atomic sensitivity factors tailored to the instrument by the manufacturer.

Solid-state ^{31}P magic angle spinning (MAS) nuclear magnetic resonance (NMR) spectra were obtained on a 9.4 T Bruker Avance® spectrometer at a resonance frequency of 161.97 MHz. Powdered samples were spun at 12 kHz in a 4 mm CP/MAS probe under ambient temperature and humidity conditions. Samples were not dried prior to examination. Spectra were acquired using a single pulse excitation pulse sequence (zg) with a 5 μs (90°) pulse length and 120 s recycle delay. The ^{31}P spin–lattice relaxation time estimated from progressive saturation experiments is ca. 30 s and does not show marked differences between the partially resolved resonance bands. ^{31}P chemical shifts were referenced to external 85% H_3PO_4 (0 ppm).

The structures of the catalysts were determined by X-ray diffraction (XRD). The XRD patterns were obtained with a Philips X'Pert Pro diffractometer equipped with a X'Celerator detector operated at 45 kV and 40 mA using Cu κα radiation (λ = 0.15406 nm) at a scan rate of 0.1° (2θ) s^{-1}.

The amounts of phosphorus, zirconium, and tin present in the solid acid catalysts were determined by elemental analysis by way of inductively coupled plasma (ICP) analysis. The samples were not degassed prior to analysis. The analyses were performed by Galbraith Laboratories, Inc.

2.3. Catalyst activity

Batch reactions were carried out in a 100 mL reactor vessel provided by Parr Instrument Company, series 4560. Glucose (Fisher Scientific) solutions were prepared with de-ionized water at the specified concentration. Throughout all of the experiments, the amount of loaded reaction solution was kept constant at 70 g.

Temperatures in the reactor were measured by means of a thermocouple in contact with the solution. All reaction solutions were mixed at a maximum constant rate of 600 rpm using an internal stirrer. The temperature and stirring were controlled by a 4848 Controller provided by Parr. The reaction vessel was initially pressurized to 800 psi with industrial grade helium (Airgas). Samples were taken periodically through a sampling port. The samples were immediately quenched in an ice water bath and filtered with a 0.2-μm syringe filter prior to analysis. The reactor was repressurized with helium after each sampling. The dip tube was covered with a stainless steel woven wire cloth, mesh size 400 × 400 provided by McMaster-Carr. This was done to prevent clogging and loss of catalyst during sampling.

2.4. Analysis

Reaction product samples were analyzed by high-pressure liquid chromatography (HPLC) with a Shimadzu© LC-20AT. Carbohydrates were detected with a RI detector (RID-10A), and reaction products were detected with a UV–Vis detector (SPD-20AV) at wavelengths of 210 and 254 nm. The column used was a Biorad© Aminex HPX-87H sugar column. The mobile phase was 0.005 M H_2SO_4 flowing at a rate of 0.6 mL/min. The column oven was set to 30 °C.

3. Results

3.1. Characterization of solid acid catalysts by adsorption and ICP

The characterization for the solid acid catalysts by adsorption and ICP appear in Table 1. Zirconia was used as a reference material due to its high Lewis acidity [71]. All of the phosphate catalysts in this study were confirmed to be amorphous by XRD (Fig. S1 in the Supplementary information). Previous studies have shown that the presence of phosphate stabilizes the amorphous zirconia phase [72]. It has also been reported that amorphous zirconium phosphate is thermally stable even after calcination at 800 °C [66]. The phosphorus to metal(IV) molar ratios obtained from ICP analysis were different than the phosphorus to metal(IV) molar ratios used in the precipitation solutions with the exception of ZrP2. The sample ZrP3 had the same phosphorus content as ZrP2 despite the additional loading of the phosphorus precursor during synthesis. The molar ratios for the two tin phosphate samples were comparable to each other, but lower than the phosphorus to tin ratio used in the prescription solution.

Zirconium phosphate samples ZrP1 and ZrP3 had similar BET surface areas to that reported by Kamiya et al. (130 $m^2 g^{-1}$) [51]. The highest surface area was obtained for ZrP2 (276 $m^2 g^{-1}$). In contrast, tin phosphate SnP1 had the lowest surface area (11 $m^2 g^{-1}$), which was appreciably lower than that reported by Patel et al. following the same preparation procedure (141 $m^2 g^{-1}$) [47].

Ammonia TPD revealed a higher concentration of total acid sites for the zirconium phosphates compared to the tin phosphate catalysts. The three zirconium phosphate samples showed similar concentrations of total acid sites as measured by NH_3-TPD (Fig. S2 in the Supplementary information). Sample ZrP2 showed the highest total acid concentration despite the equivalent P/Zr molar ratios to sample ZrP3. This higher total acid concentration for ZrP2 could be due to its higher surface area. SnP1 had a comparable acid concentration to that reported in the literature [47]. In contrast, an increased amount of acid sites was observed for SnP2 despite the similar amounts of phosphorus incorporated in the framework. The two tin phosphate samples showed similar acid strength according to the NH_3-TPD profiles.

Brønsted acid sites were quantified according to isopropylamine TPD [68–70]. The concentrations of Brønsted acid sites obtained for the zirconium phosphate samples were at least 3 times higher than the concentration of Brønsted acid sites for the tin phosphates (Fig. S3 in the Supplementary information). ZrP2 showed the highest Brønsted acid concentration among all of the catalysts tested, containing more than 26 times the amount of Brønsted sites observed with SnP1. In this respect, extensive studies have been reported on the use of ^{1}H MAS NMR spectroscopy to determine the strength of Brønsted acid sites. Acid sites of increasing acid strength are characterized by higher ^{1}H NMR chemical shifts [73]. Fraissard and co-workers have measured the acid strength of several types of acid catalysts by two ^{1}H NMR techniques in the presence of water [74–79]. As part of this study, the zirconium phosphate samples were characterized by solid-state ^{1}H MAS NMR spectroscopy. Results reveal that all three samples showed a broad resonance at 7.3 ppm. The placement is downfield of the shift for water (4.8 ppm) and represents a weighted average of the acid proton chemical shifts and water [77]. The chemical shift of all three materials is the same implying that their acid strengths are comparable. This corresponds with results obtained from NH_3-TPD. It is also notable to mention that the fraction of Brønsted acid sites for ZrP2 in this study was somewhat lower than that reported by us in our previous study [40]. This could be due to a number of factors including differences in the catalyst washing routine during the synthesis procedure or different characterization techniques. NH_3 FT-IR spectroscopy was used to quantify the ratio of Brønsted to Lewis sites in our previous study. Isopropylamine TPD was used in this study. This could also lead to inconsistencies in the quantification of the Brønsted acid sites by different techniques, as different adsorption techniques quantify sites differently.

3.2. Solid-state ^{31}P MAS NMR spectroscopy

The zirconium phosphate samples were characterized by solid-state ^{31}P MAS NMR spectroscopy. This characterization method serves as a useful technique to identify the coordination states of the phosphorus atoms in the bulk phase. Generally, a transition

Table 1
Characterization of solid acid catalysts by adsorption and ICP studies.

Catalyst	BET surface area[a] ($m^2 g^{-1}$)	Metal(IV)[b] (molar%)	Phosphorus[b] (molar%)	P/metal(IV) molar ratio	Total acid sites[c] (mmol g^{-1})	Brønsted acid sites[d] (mmol g^{-1})	Fraction of Brønsted acid sites
ZrP1	173	9.45	12.07	1.28	1.942	0.240	0.12
ZrP2	276	8.29	16.60	2.00	2.146	0.818	0.38
ZrP3	123	8.07	15.95	1.98	1.834	0.388	0.21
SnP1	11	9.20	6.64	0.72	0.463	0.031	0.07
SnP2	142	11.03	7.20	0.65	1.260	0.068	0.05
ZrO_2	143	–	N/A	N/A	0.905	0.087	0.10

[a] BET "C" constants for the catalysts in descending order are 88, 89, 73, 44, 185, and 80.
[b] Determined from elemental analysis (Galbraith Laboratories, Inc.).
[c] Determined from ammonia TPD.
[d] Determined from isopropylamine TPD.

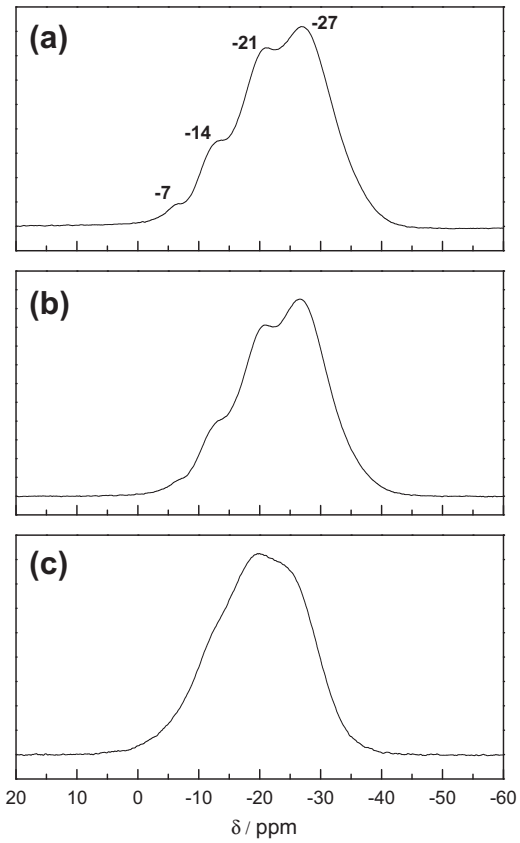

Fig. 2. Solid-state ^{31}P MAS NMR spectra of the zirconium phosphate catalysts: (a) ZrP3, (b) ZrP2, and (c) ZrP1.

of the chemical shift (δ_P) to more negative values is indicative of both an increase in the number of P–O–Zr bonds [80,81], as well as an increase in the chain length of the phosphorus atoms [67]. The latter corresponds to progressive deprotonation and subsequent condensation of phosphate species (P–O–P bonds), typically during calcination [80]. Fig. 2 shows the NMR spectra for the three zirconium phosphate samples. All of the samples showed relatively broad peaks due to their amorphous nature [66,82]. Samples ZrP2 and ZrP3 showed very similar spectra which were characterized by four different resonance peaks. The resonance peak at −7 ppm is attributed to tetrahedral phosphates bonded to one zirconia group and two hydroxyl groups (Zr–O)–PO(OH)$_2$. This coordination gives way to geminal P-(OH) groups. The signal at −14 ppm signifies the presence of two zirconia and one hydroxyl group bonded to the phosphate (Zr–O)$_2$–PO(OH). Similarly, a peak at −21 ppm can be assigned to a tetrahedral phosphate connected with three zirconia groups (Zr–O)$_3$–PO. The high intensity peak at −27 ppm implies relatively high amounts of polyphosphates, P–O–P, due to condensation of phosphate species [54,66]. The resonance peaks associated with zirconium phosphate ZrP1 were broader and less discrete than those for the other two samples.

The NMR spectra were deconvoluted using Origin software. The four resonance bands were fit with Gaussian line shapes. The band areas were normalized according to the sample weight, assuming equal density for the samples. Table 2 shows the relative amounts of the different phosphate species for each catalyst. The spectrum of ZrP1 has just three inflections and gave unreasonable fitting results until (Zr–O)–PO(OH)$_2$ was constrained to a small value. Overall, from these results, it can be concluded that ZrP2 and ZrP3 are quite similar materials with respect to their bulk properties. In contrast, ZrP1 showed a higher amount of (Zr–O)$_2$–PO(OH) species at −14 ppm and less polyphosphates at −27 ppm compared to ZrP2 and ZrP3. Panda et al. reasoned that the Brønsted acid sites in their study of mesoporous zirconium phosphate came primarily from geminal P(OH) groups [66]. This corresponds to the coordination state detected at −7 ppm. Others have postulated that the Brønsted acid sites come from the phosphate species on the surface bonded to two and three zirconia groups (chemical shifts −14 ppm and −21 ppm, respectively) [81,83]. It is unlikely that these former conclusions are valid for this study, as the samples with the highest concentration of Brønsted acid sites (ZrP2 and ZrP3) are predominantly comprised of polyphosphate species. Consequently, even though the formation of polyphosphates species is attributed with deprotonation, their increased amount in the bulk phase could be a primary cause of the higher Brønsted acidity observed for ZrP2 and ZrP3 in relation to ZrP1. According to Segawa et al., P–O–P species in the bulk phase can withdraw electrons from the residual phosphate groups on the surface, thus enhancing the acidic properties of P–OH groups on the surface [84,85].

3.3. XPS analysis

The zirconium phosphate catalysts were characterized by XPS in order to study their surface composition and oxidation states. Fig. 3 shows the high resolution XPS spectra of zirconium, phosphorus, and oxygen for the three zirconium phosphate catalysts. The Zr*3d* line is composed of two peaks assigned to Zr$3d_{5/2}$ at 183 eV and Zr$3d_{3/2}$ at roughly 185 eV. This is characteristic of tetravalent zirconium Zr^{4+} [86]. All samples had typical P*2p* binding energies of 133 eV, characteristic of pentavalent tetracoordinated phosphorus (P^{5+}) [86,87]. The O*1s* line shows a broad peak which could correspond to oxygen bonded to both zirconium and phosphorus [86]. The O*1s* component characteristic of the P–O bond

Table 2
Relative amounts of the different phosphate species for the zirconium phosphate catalysts from solid-state ^{31}P MAS NMR spectroscopy.

Chemical shift (ppm)	−7	−14	−21	−27
Coordination state[a]	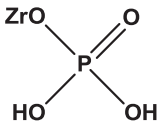	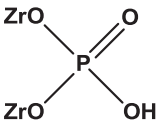	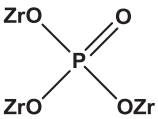	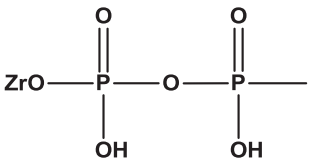
Catalyst	Relative amount (%)			
ZrP1	2.3[b]	30.9	15.7	51.1
ZrP2	3.6	12.9	11.8	71.7
ZrP3	5.0	11.3	13.5	70.2

[a] Adapted from Ref. [66].
[b] This value was constrained. Any small value is acceptable.

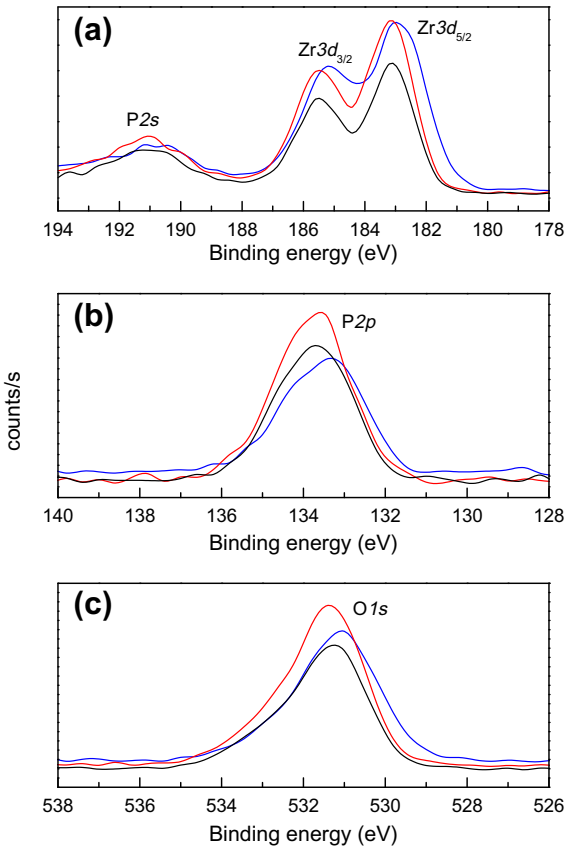

Fig. 3. High-resolution XPS spectra of the (a) Zr*3d*, (b) P*2p*, and (c) O*1s* regions for the catalysts: ZrP1 (—); ZrP2 (—); ZrP3 (—).

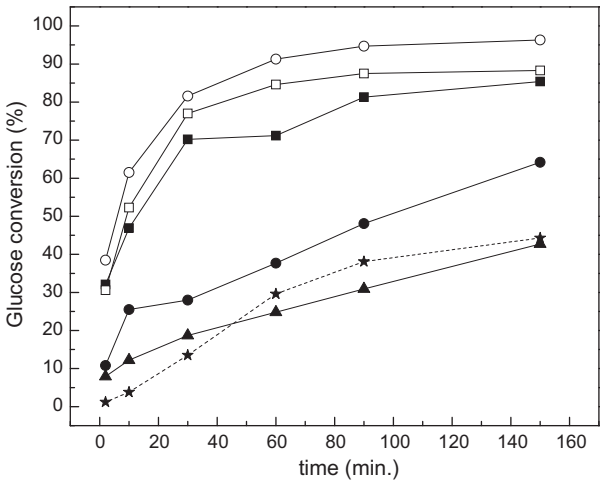

Fig. 4. Aqueous phase glucose dehydration at 160 °C in a stirred batch reactor with different solid acid catalysts. Feed was 10 wt.% glucose aqueous solution. The solid catalyst loading was constant at 5 wt.%. Catalysts: ZrP1 (■), ZrP2 (●), ZrP3 (▲), SnP1 (□), SnP2 (○). Blank run (dashed line) (★).

is dominant for all samples with an average binding energy of 531 eV.

The surface atomic compositions of the zirconium phosphate catalysts appear in Table 3. These values were determined by the XPS line areas of Zr*3d*, P*2p*, and O*1s*, and the phosphorus to zirconium atomic ratios on the surface were calculated accordingly. There is a gradual increase in phosphorus on the surface in agreement with the increase in phosphorus loading in the preparation procedure. The P/Zr molar ratio on the surface increased as follows: ZrP1 < ZrP2 < ZrP3. The atomic compositions on the surfaces showed only slight differences to the bulk compositions (see Tables 1 and 3). Catalyst ZrP1 showed practically identical P/Zr surface and bulk molar ratios, as determined by XPS and ICP, respectively. However, higher zirconium and phosphorus contents were observed on the surface than in the bulk (Table 1). The relatively higher amount of zirconium on the surface of ZrP1 could be a plausible cause for its relatively higher concentration of Lewis acid sites compared to ZrP2 and ZrP3. For sample ZrP2, the phosphorus content on the surface was slightly lower than in the bulk. The opposite trend was found for zirconium. The highest P/Zr molar ratio on the surface was observed for ZrP3. Nevertheless, this value was lower than the theoretical ratio predetermined in the preparation procedure (P/Zr = 3).

Electron binding energy shifts observed for Zr, P, and O can reflect variations in the polarity of the bonds on the surface of zirconium phosphate catalysts. A slight downward shift in the Zr*3d* binding energies was observed for sample ZrP1 compared to ZrP2 and ZrP3. This indicates a reduced polarization of the Zr–O bonds in the ZrP1 sample, which could be due to fewer hydroxyl groups on the surface relative to the other samples [88]. As for the P*2p* binding energies, the shifts increased as follows: ZrP1 < ZrP2 < ZrP3. Higher P*2p* binding energies are a result of increased polarity of the P–O bonds on the surface which can be enhanced by the hydroxyl groups bonded to the phosphorus atoms [88]. This suggests that higher P*2p* binding energies are indicative of increased amounts of acid sites on the surface, as shown with ZrP2 and ZrP3. The O*1s* binding energies increase according to: ZrP1 < ZrP3 < ZrP2. Higher O*1s* binding energy suggests an increased amount of surface hydroxyl groups [88].

3.4. Aqueous phase glucose dehydration studies with solid metal(IV) phosphate catalysts

Glucose dehydration studies were carried out at 160 °C with the different solid acid catalysts in the aqueous phase. The concentration of the catalysts was kept constant at 5 wt.%. Fig. 4 depicts glucose conversion as a function of reaction time for the various catalysts. The tin phosphate catalysts showed a higher activity compared to the zirconium phosphate catalysts. As part of this study, a run without any catalyst was also carried out and showed that glucose underwent hydrothermal decomposition. Similar observations were noted in our previous study where we studied the kinetics of levulinic acid production from

Table 3
Electron binding energies and atomic surface composition determined by XPS for the zirconium phosphate catalysts.

Catalyst	Binding energy (eV)				Surface atomic composition[a] (%)			P/Zr molar ratio
	Zr$3d_{3/2}$	Zr$3d_{5/2}$	P*2p*	O*1s*	Zr	P	O	
ZrP1	185.2	183.0	133.3	531.1	11.1	13.6	75.3	1.26
ZrP2	185.5	183.1	133.6	531.4	8.8	16.3	75.0	1.85
ZrP3	185.5	183.1	133.7	531.3	8.1	16.6	75.2	2.05

[a] Based on XPS line areas of Zr*3d*, P*2p* and O*1s*.

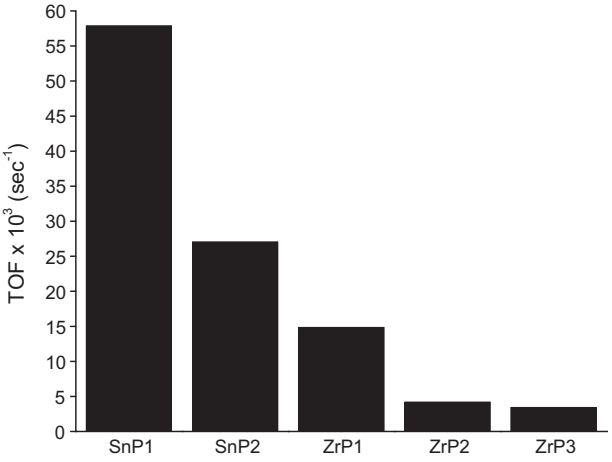

Fig. 5. Aqueous phase glucose dehydration at 160 °C in a stirred batch reactor. Initial turn-over frequency (according to total acid sites concentration determined from NH_3-TPD) based on glucose disappearance for the different solid acid catalysts. Feed was 10 wt.% glucose aqueous solution. The solid catalyst loading was constant at 5 wt.%. The homogeneous glucose reactions were subtracted out for calculation purposes.

glucose [26]. There we found that nearly full glucose disappearance was attained at 180 °C after 150 min. without an acid catalyst, and 75% of the overall carbon content went to form water soluble and insoluble humic species. In this study, the catalyst activity obtained from sample ZrP3 was lower than that from the hydrothermal reactions with glucose at longer reaction times. This suggests that zirconium phosphate suppresses some of the undesired reactions encountered under hydrothermal conditions. Fig. 5 shows the initial turnover frequency (TOF) of glucose disappearance for the different catalysts in this study. The TOF calculations are based on the total concentration of acid sites as determined by NH_3-TPD. On a per site basis, the catalytic activity increased as follows: ZrP3 < ZrP2 < ZrP1 < SnP2 < SnP1. As mentioned previously, results from the NH_3-TPD and ^1H MAS NMR studies showed that the acid strengths for each series of metal(IV) phosphates were similar. Therefore, it is reasonable to assume that acid strength does not play a significant role in determining the catalyst activity. For calculation purposes, the homogeneous (blank) glucose reactions were subtracted out of the TOF estimations.

Fig. 6 shows the carbon selectivities of the major products as a function of glucose conversion. The tin phosphate catalysts had a higher fructose selectivity compared to the zirconium phosphates, as shown in Fig. 6a. This is in agreement with the work of Davis and co-workers [31–33] and Dumesic and co-workers [34,35,89], where they find that Lewis acid sites catalyze the isomerization reaction of glucose to fructose. The fructose selectivity increased as follows: blank < ZrP3 < ZrP2 < ZrP1 < SnP1 ∼ SnP2. In all cases, the fructose selectivity decreased with increased glucose conversion. It is notable to mention that lactic acid was also detected as a by-product of this reaction. The amounts were not quantified, but were observed for all of the solid catalysts tested here due to the presence of Lewis acid sites. Recently, Chambon et al. published a study on the production of lactic acid from cellulose with solid Lewis acid catalysts [90]. They found that Lewis sites improve the extent of cellulose depolymerization compared to Brønsted acid sties. Holm et al. also recently discovered that solid Lewis acid catalysts, such as Sn-Beta, are able to convert pentose and hexose sugars to methyl lactate in methanol [89,91].

Fig. 6b depicts the HMF selectivity for the different metal(IV) phosphates. Initially, the HMF selectivity increased as it was

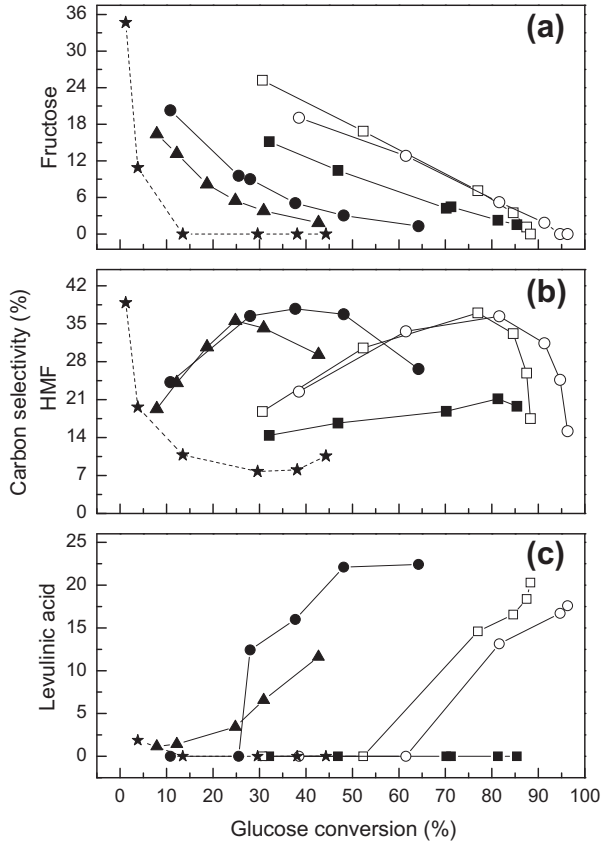

Fig. 6. Carbon selectivity of major products as a function of glucose conversion for different metal phosphate catalysts at 160 °C: (a) fructose, (b) HMF, and (c) levulinic acid. Feed was 10 wt.% glucose aqueous solution. The solid catalyst loading was constant at 5 wt.%. Catalysts: ZrP1 (■), ZrP2 (●), ZrP3 (▲), SnP1 (□), SnP2 (○). Blank run (dashed line) (★).

being produced from glucose and fructose. The HMF selectivity then decreased as it reacted to produce levulinic acid, formic acid, and decomposition products. Higher HMF selectivities were observed for ZrP2 and ZrP3 at relatively low glucose conversions. This coincides with the trend that was observed for catalysts with relatively high Brønsted to Lewis ratios [40]. The HMF selectivity reached a maximum of 38% with ZrP2 at a glucose conversion of 38%. Similar selectivities were achieved with the tin phosphate catalysts at a glucose conversion of 80%. The lowest selectivity was observed for non-catalyzed glucose decomposition (blank run).

A relatively high levulinic acid selectivity was observed for the zirconium phosphate catalysts ZrP2 and ZrP3 compared to the tin phosphates, as shown in Fig. 6c. For the tin phosphates, levulinic acid was detected only at glucose conversions above 80%. The catalyst ZrP2 showed the highest levulinic acid selectivity of 22% at a glucose conversion of 64%. In contrast, catalyst ZrP1 showed no production of levulinic acid. No levulinic acid was observed when only water was used. The levulinic acid selectivity increased as follows: blank ∼ ZrP1 < SnP2 < SnP1 < ZrP3 < ZrP2. In all cases, the levulinic acid selectivity increased with increasing glucose conversion.

In addition to the major products mentioned earlier, quantifiable amounts of cellobiose, levoglucosan, and furfural were also detected as by-products for all of the catalysts tested in this study. Cellobiose was detected primarily for catalysts with relatively high Brønsted to Lewis ratios, such as ZrP2 and ZrP3. Carbon selectivity to cellobiose decreased with glucose conversion. The maximum carbon selectivity was 36% at 8% glucose conversion for ZrP3.

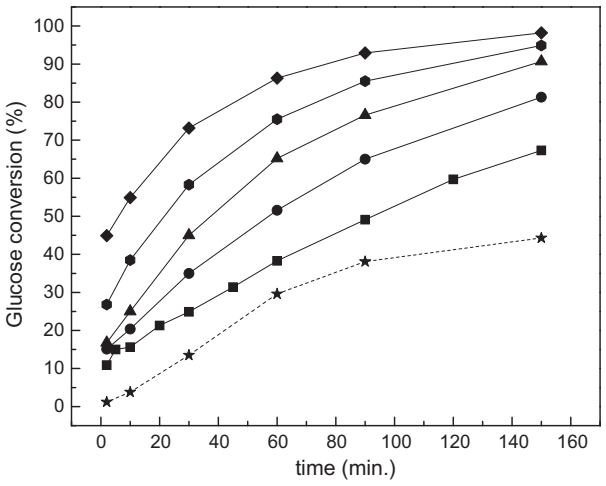

Fig. 7. Aqueous phase glucose dehydration in a stirred batch reactor. Effect of the Brønsted to Lewis acid ratio on glucose conversion with homogeneous acid catalysts at 160 °C. Feed was 10 wt.% glucose aqueous solution. Total acid concentration was kept constant at 0.1 M. Brønsted to Lewis acid ratio = 1:0 (■), 3:1 (●), 1:1 (▲), 1:3 (⬢), and 0:1 (◆). Blank run (dashed line) (★).

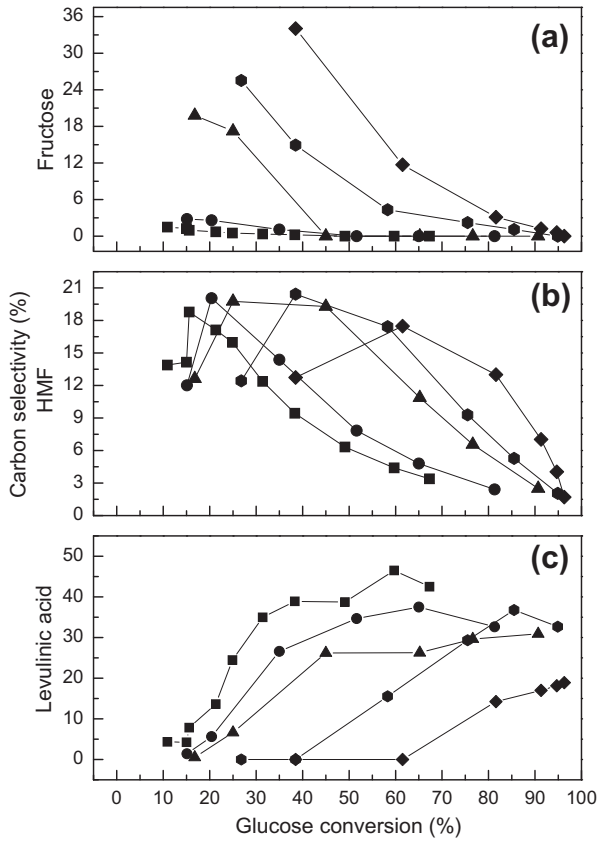

Fig. 8. Effect of the Brønsted to Lewis acid ratio on the carbon selectivity of major products from glucose dehydration with homogeneous acid catalysts at 160 °C: (a) fructose, (b) HMF, and (c) levulinic acid. Feed was 10 wt.% glucose aqueous solution. Total acid concentration was kept constant at 0.1 M. Brønsted to Lewis acid ratio = 1:0 (■), 3:1 (●), 1:1 (▲), 1:3 (⬢), and 0:1 (◆).

Similar trends were observed for levoglucosan with a maximum carbon selectivity of 13% at 8% at glucose conversion for ZrP3. Furfural was also detected, but at carbon selectivities no higher than 4%. Higher selectivities to furfural were observed for catalysts with higher amounts of Lewis acid sites.

3.5. Aqueous phase dehydration of glucose with homogeneous acid catalysts

Aqueous phase glucose dehydration studies were carried out with water-soluble Lewis and Brønsted acids. Ytterbium(III) trifluoromethanesulfonate hydrate, $Yb(OTf)_3$, and hydrochloric acid were used, respectively. The former is considered a stable water-soluble Lewis acid [92,93]. Reactions were performed at varying Brønsted to Lewis ratios by combining the two acids accordingly, while holding the total acid concentration constant at 0.1 M. Fig. 7 shows the results of glucose conversion for the different ratios of the homogeneous catalysts. The activity for glucose disappearance increased systematically as the relative amount of Lewis sites increased. Pure $Yb(OTf)_3$ showed the highest glucose conversion, whereas pure HCl had the lowest catalytic activity. These results indicate that the Lewis acid sites have a higher catalytic activity toward glucose disappearance compared to the Brønsted acid sites, which is consistent with the results from the heterogeneous catalysts.

Fig. 8 depicts the carbon selectivities of the major compounds as a function of glucose conversion for the various Brønsted to Lewis ratios in the homogeneous regime. The selectivity for fructose production increased with the concentration of Lewis sites, as shown in Fig. 8a, reaching a maximum of 34% at 45% conversion with pure $Yb(OTf)_3$ as a catalyst. Fig. 8b shows the HMF selectivity for the different Brønsted to Lewis ratios in the homogeneous regime. As with the solid acid catalysts, a maximum selectivity was observed for all ratios. This maximum value shifts toward higher glucose conversions as the relative amount of Lewis acid sites increases. At lower glucose conversions, HMF was selectively produced by catalysts with more Brønsted acid sites. Lewis acid sites showed a higher selectivity for HMF production at higher glucose conversions. The selectivity toward levulinic acid production from glucose systematically increases with the concentration of Brønsted sites, as depicted in Fig. 8c. Pure HCl showed a significantly higher levulinic acid selectivity compared to $Yb(OTf)_3$, with a maximum selectivity of 46% at 60% glucose conversion. These results are consistent with those reported for the heterogeneous catalysts.

4. Discussion

The reaction chemistry for levulinic acid production from glucose consists of three key steps. Glucose undergoes isomerization to produce fructose and mannose; hexoses undergo dehydration to form HMF, and HMF undergoes a rehydration reaction to produce levulinic acid and formic acid. Additional undesirable decomposition reactions can also come about from glucose, fructose, and HMF to ultimately form humins. For this study, humins were considered as all unidentified water soluble and insoluble compounds. Further characterization of humic species was not carried out in this study, as this goes beyond the scope of this paper. Table 4 shows the product distribution of all identified products for the metal(IV) phosphates. The values were interpolated to correspond with a glucose conversion of 40%. The results show that the formation of humins was predominant for the reaction with ZrP1. The catalyst ZrP2 showed the lowest selectivity toward these undesired compounds, which is consistent with its high selectivity toward HMF and levulinic acid. The tin phosphate catalysts showed similar trends to each other for humins formation. Following the reactions in this study, it was observed that solid humins were deposited on all of the solid acid catalysts. This was also noticed in our recent study with ZrP for cellulose decomposition [43]. The amounts of carbon deposited on the catalysts were not determined, and regeneration was not carried out in this publication.

Table 4
Product distribution at 40% glucose conversion for the metal(IV) phosphate catalysts at 160 °C. Feed was 10 wt.% glucose aqueous solution. The solid catalyst loading was constant at 5 wt.%.

Catalyst	Carbon selectivity (%)							
	Fructose	Cellobiose	Levoglucosan	HMF	Furfural	Levulinic acid	Formic acid	Humins[a]
ZrP1	12.6	1.8	0.6	15.6	2.3	0.0	4.1	63.0
ZrP2	4.6	6.2	3.8	37.5	1.5	17.3	5.4	23.7
ZrP3	2.3	6.3	4.0	30.4	1.0	10.5	3.9	41.6
SnP1	21.6	3.7	1.7	23.9	2.4	0.0	1.2	45.5
SnP2	18.7	3.3	1.4	23.2	2.2	0.0	1.8	49.4

[a] Considered all unidentified water soluble and insoluble products.

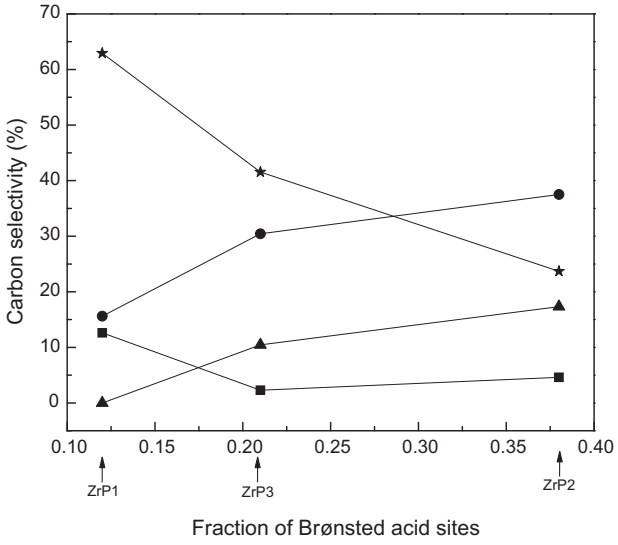

Fig. 9. Carbon selectivity of major products at 40% glucose conversion as a function of the concentration of Brønsted acid sites (determined by isopropylamine TPD) for the zirconium phosphate catalysts at 160 °C. Feed was 10 wt.% glucose aqueous solution. The solid catalyst loading was constant at 5 wt.%. Major products: fructose (■), HMF (●), levulinic acid (▲), humins (★).

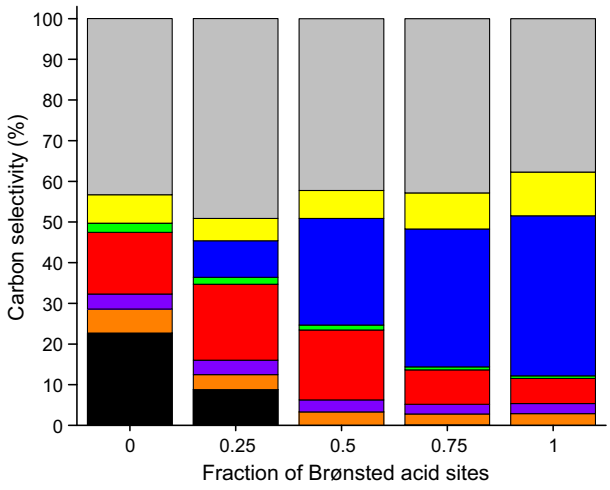

Fig. 10. Carbon selectivity of water-soluble products as a function of the fraction of Brønsted acid sites for the homogeneous acid catalysts at 50% glucose conversion and 160 °C. Total acid concentration was kept constant at 0.1 M. Feed was 10 wt.% glucose aqueous solution. ■ fructose; ■ cellobiose; ■ levoglucosan; ■ HMF; ■ furfural; ■ levulinic acid; ■ formic acid; ■ humins.

However, we have shown in our previous studies that we can obtain a satisfactory carbon balance for these aqueous dehydration reactions based on various characterization techniques [26,43]. This indicates that the method used in this study to calculate the product selectivities is valid.

Fig. 9 shows the carbon selectivity of the major products as a function of the fraction of Brønsted acid sites for the three zirconium phosphate catalysts. The values were interpolated to correspond with a glucose conversion of 40%. There is a direct correlation between the product distribution and the fraction of Brønsted sites as determined by TPD measurements with ammonia and isopropylamine. HMF and levulinic acid production increase with the amount of Brønsted acid sites. Isomerization to produce fructose from glucose is predominant at higher Lewis acid concentrations, as shown for sample ZrP1. The formation of humic species is greatest at lower Brønsted to Lewis ratios. Consequently, a higher rate of glucose disappearance and lower selectivities to HMF and levulinic acid are observed for catalysts with increased Lewis sites.

This claim is further supported by the studies carried out with homogeneous Brønsted and Lewis acid catalysts. Fig. 10 shows the carbon selectivities of all the identified products as a function of the fraction of Brønsted acid sites for the homogeneous acid catalysts. These calculated values were interpolated to correspond with a glucose conversion of 50%. Levulinic acid and formic acid selectivities increase as the fraction of Brønsted sites increases. A minimal HMF selectivity is observed with pure Brønsted acid sites suggesting this type of acid site predominantly catalyzes the rehydration of HMF to form levulinic acid and formic acid. In contrast, Lewis acid sites favor the isomerization reaction of glucose to fructose. Similar conclusions have been reported in the past by Davis and co-workers in their studies of tin-containing zeolites as highly active solid Lewis acid catalysts [31–33] and by Dumesic and Shanks [34,35]. As with the dehydration step, it is apparent from the results that both Brønsted and Lewis acid sites catalyze the production of HMF from glucose and fructose, reaching a maximum carbon selectivity of 19% at 50% glucose conversion with a Brønsted acid site fraction of 0.25. The selectivity to humins does not vary much as a function of the Brønsted to Lewis acid site ratio; however, a slight decrease is observed at higher fractions of Brønsted sites.

Two classes of metal(IV) phosphates have been prepared based on tin and zirconium precursors. Despite the same phosphorus to metal(IV) molar loadings in the preparation procedure, the tin phosphates have lower phosphorus concentrations than the zirconium phosphates according to elemental analysis. The phosphorus to metal(IV) ratios obtained for the zirconium phosphates are more than two fold the amount obtained for the tin-based analogs. Consequently, the zirconium phosphates all have higher total acid and Brønsted acid concentrations according to ammonia and isopropylamine TPD, respectively. Prior studies which have compared different types of metal(IV) phosphates have reported conflicting results. Patel et al. [47,50] compared tin, zirconium, and titanium phosphates for cyclodehydration of 1,*n*-diols. They found tin phosphate to be the most active and selective catalyst, which they attributed to its relatively high surface area and strong acid sites. Similar

conclusions were deduced by Gu et al. [59] in their study of sorbitol dehydration to produce isosorbide. It is notable to mention that the catalysts tested in these previous studies were not calcined. The discrepancy with our study could be attributed to the differences in catalyst preparation procedures. Similarly, Tran et al. have shown a direct correlation between the acidic and catalytic properties of sulfated zirconia and its calcination temperature [94]. It has been reported in the literature that the concentration of Brønsted acid sites for crystalline zirconium phosphate is maximized at a calcination temperature of 400 °C [65].

The bulk and surface properties of the zirconium phosphate catalysts differ according to their phosphorus loadings. Results from elemental analysis and ^{31}P solid-state NMR spectroscopy show that catalysts ZrP2 and ZrP3 are quite similar in the bulk phase. Despite the different phosphorus loadings in the preparation procedure, both catalysts contain nearly identical phosphorus amounts in the bulk phase, as well as on the surface. The highest attainable phosphorus to zirconium molar ratio is 2:1. This is similar to the maximum P/Zr ratio of 2.21 reported by Sinhamahapatra et al. who studied the effect of phosphate concentration and calcination temperature on the catalytic properties of mesoporous zirconium phosphate [66].

Characterization techniques carried out in this study show noticeable differences in surface properties among the three zirconium phosphate catalysts. As shown with ZrP1 and ZrP2, increased phosphorus loading results in higher phosphorus content in the bulk and on the surface. This in turn increases the total acidity and Brønsted acidity [66]. Conversely, a higher zirconium loading increases the Lewis acidity due to increased amounts of tetravalent zirconium (Zr^{4+}), as shown for ZrP1. Further increasing the phosphorus loading in the preparation step from a P/Zr molar ratio of 2 to 3 does not increase the phosphorus content in the bulk or on the surface, as shown for ZrP2 and ZrP3. Among the three zirconium phosphate catalysts, ZrP2 has the highest surface area, as well as the highest overall acid and Brønsted acid concentrations. Consequently, ZrP2 was found to contain the highest amount of hydroxyl groups on its surface, as confirmed with XPS analyses. This could explain its high concentration of Brønsted acid sites [44]. Kellum and Hahn found a direct correlation between the concentration of surface hydroxyl groups and the surface area for a series of trimethylsiloxy-treated ammonium silicates [95]. Therefore, the increased amount of surface hydroxyl groups on ZrP2 could also be a cause for its relatively high surface area. On the other hand, other studies have claimed that the preparation conditions have a strong effect on the structure and surface properties of zirconia catalysts. Specifically, the nature of the zirconium precursor, the pH of the solution during precipitation, temperature and time of digestion, and calcination temperature all play key roles that influence these properties [96–99]. In this study, the zirconium phosphate catalysts differ by the P/Zr molar ratios in the preparation step. This was achieved by varying the relative amounts of phosphorus and zirconium precursors (ammonium phosphate monobasic and zirconium oxychloride octahydrate, respectively). This in turn alters the pH of the solution during precipitation, which could be a cause for varying surface areas observed for the different samples.

Various groups have studied the effect of phosphate and sulfate loading on different acid catalysts. Sinhamahapatra et al. discovered that a phosphate to zirconium ratio of 2 yields the highest surface area as well as the highest concentration of total acid sites and Brønsted acid sites as determined by NH_3-TPD and DRIFTS spectra for pyridine adsorption, respectively [66]. A further increase in phosphate loading (P/Zr ratio 3) resulted in a decrease in total acidity and Brønsted acidity. They reasoned the decrease in Brønsted acidity was due to the formation of polyphosphate, which in turn diminishes the P–OH groups. It is unlikely that these conclusions are entirely valid for this study, as the relative amounts of the polyphosphate species for ZrP2 and ZrP3 are nearly identical (Table 2), whereas ZrP2 shows a higher concentration of acid sites compared to ZrP3. However, it has been reported in the literature that the length of the polyphosphate chain is a function of the metal oxide to phosphate ratio [100]. An increase in the polyphosphate chain length is observed with increased amounts of P_2O_5. Determining the composition and chain length of the polyphosphate species was not a focus of this study; however, differences in these parameters between ZrP2 and ZrP3 could be a reason for the discrepancies in their catalytic properties. Determining the optimal phosphate species for this reaction is beyond the scope of this paper and will be the focus of future studies. Another analogous study was reported by Mishra and Parida who examined the effect of sulfate loading on sulfated zirconia catalysts [71]. According to their results, increasing the sulfate loading from 10 wt.% to 15 wt.% resulted in decreased sulfur content as determined by elemental analysis. The increase in sulfate loading also resulted in inferior catalytic properties including lower surface area, lower overall acidity, and decreased surface hydrophilicity. Another study was carried out by Ahmed et al. on the effect of sulfate loading with sulfated zirconia [101]. They incorporated SO_4^{2-} in zirconia ranging from 5 to 30 wt.% and found the catalyst with a loading of 15 wt.% sulfate to possess the highest surface area, as well as highest total acidity and Brønsted to Lewis ratio. Consequently, this catalyst was found to exhibit optimal catalytic activity for ethanol dehydration.

5. Conclusions

We have prepared and characterized a series of metal(IV) phosphate catalysts and tested them for aqueous phase dehydration of glucose to levulinic acid. Adsorption studies with ammonia and isopropylamine as probe molecules reveal a higher overall concentration of acid sites for the zirconium phosphates compared to the tin phosphate catalysts. Sample ZrP2 shows the highest amount of total acid sites, as well as the highest concentration of Brønsted sites among all of the catalysts tested. XPS analysis corroborates these findings by revealing a high concentration of surface hydroxyl groups for the zirconium phosphate catalysts, specifically ZrP2. Four phosphorus coordination states have been identified by solid-state ^{31}P MAS NMR spectroscopy, among which the polyphosphate species has the highest relative amount. The higher amounts of polyphosphate species detected in ZrP2 and ZrP3 could be a reason for its enhanced acidity compared to ZrP1. Likewise, the length of the polyphosphate chain could also play a key role in determining the concentration of the acid sites.

We have demonstrated here that both heterogeneous and homogeneous Lewis and Brønsted sites share different functions as related to the proposed reaction scheme for glucose dehydration. The catalytic activity and selectivity for all of the metal(IV) phosphates tested in this study vary according to the Brønsted to Lewis ratio. Catalysts with high Lewis acidity, such as the tin phosphates, show the highest activity on a per site basis, whereas the zirconium phosphates with relatively high Brønsted acidity (i.e. ZrP2 and ZrP3) demonstrate the lowest activity. Fructose selectivity increases with an increase in the Lewis acid concentration of the catalyst. This is due to induced isomerization reaction catalyzed by Lewis acid sites. Both types of acid sites catalyze the dehydration reaction to produce HMF from glucose. However, the HMF selectivity increases with increased concentration of Brønsted acid sites, particularly at lower glucose conversions for the heterogeneous catalyst. The levulinic acid selectivity is also a function of the relative concentration of Brønsted to Lewis sites. The levulinic acid selectivity increases with an increase in the Brønsted to Lewis

ratio for both the heterogeneous and homogeneous acid catalysts. The formation of humic species increases with increased Lewis acidity for the heterogeneous catalysts.

Increase in the P/metal(IV) molar ratio from 1 to 2 in the precursor solution results in a higher surface area, as well as increased overall concentration of acid sites and Brønsted acid sites. However, for the tin phosphates, the fraction of Brønsted sites remains the same for both catalysts in the series (SnP1 and SnP2). Consequently, both catalysts show nearly identical selectivities for the major reaction products. For the zirconium phosphates, a further increase in phosphorus loading to a P/Zr molar ratio of 3 does not alter the bulk phase of the catalyst, rather only the surface properties. Moreover, all three zirconium phosphates are predominantly comprised of phosphate species in the polyphosphate form.

Among the zirconium phosphate catalysts, the catalyst with a P/Zr ratio of 2 (ZrP2) exhibits the highest surface area, as well as the highest amount of total acid sites and fraction of Brønsted sites. This catalyst in turn exhibits the highest selectivity to HMF and levulinic acid production. A relatively high concentration of surface hydroxyl groups is most likely the source of the relatively high amounts of Brønsted acid sites, as well as the high surface area. Differences in preparation conditions, such as pH, could also lead to variations in the surface properties, as well as deviations in the composition of the phosphate species in the bulk. This study lays the grounds for further design of improved hydrothermally stable solid acid catalysts displaying high activity and selectivity to HMF and levulinic acid from carbohydrates.

Acknowledgments

This material is based upon work supported as part of the Institute for Atom-efficient Chemical Transformations (IACT), an Energy Frontier Research Center funded by the US Department of Energy, Office of Science, Office of Basic Energy Sciences. The authors would also like to gratefully acknowledge financial support from NSF-CBET (Grant # 0756663) and NSF MRI (Grant # 0722802). We also sincerely thank Jacob Hirsch from the Department of Polymer Science and Engineering at the University of Massachusetts–Amherst for performing the XPS measurements and the data analysis.

Appendix A. Supplementary material

Supplementary data associated with this article can be found, in the online version, at http://dx.doi.org/10.1016/j.jcat.2013.03.023.

References

[1] G.W. Huber, J.A. Dumesic, Catal. Today 111 (2006) 119–132.
[2] L.R. Lynd, J.H. Cushman, R.J. Nichols, C.E. Wyman, Science 251 (1991) 1318–1323.
[3] R.R. Davda, J.W. Shabaker, G.W. Huber, R.D. Cortright, J.A. Dumesic, Appl. Catal. B 56 (2005) 171–186.
[4] J.N. Chheda, J.A. Dumesic, Catal. Today 123 (2007) 59–70.
[5] J.N. Chheda, G.W. Huber, J.A. Dumesic, Angew. Chem. Int. Ed. 46 (2007) 7164–7183.
[6] D.A. Simonetti, J.A. Dumesic, ChemSusChem 1 (2008) 725–733.
[7] D.A. Simonetti, J.A. Dumesic, Catal. Rev. 51 (2009) 441–484.
[8] D.M. Alonso, J.Q. Bond, J.A. Dumesic, Green Chem. 12 (2010) 1493–1513.
[9] J.C. Serrano-Ruiz, R.M. West, J.A. Dumesic, Annu. Rev. Chem. Biomol. Eng. 1 (2010) 79–100.
[10] J.C. Serrano-Ruiz, J.A. Dumesic, Energy Environ. Sci. 4 (2011) 83–99.
[11] G.W. Huber, S. Iborra, A. Corma, Chem. Rev. 106 (2006) 4044–4098.
[12] L. Petrus, M.A. Noordermeer, Green Chem. 8 (2006) 861–867.
[13] A. Corma, S. Iborra, A. Velty, Chem. Rev. 107 (2007) 2411–2502.
[14] J.J. Bozell, L. Moens, D.C. Elliott, Y. Wang, G.G. Neuenscwander, S.W. Fitzpatrick, R.J. Bilski, J.L. Jarnefeld, Resour. Conserv. Recycl. 28 (2000) 227–239.
[15] P. Gullón, A. Romaní, C. Vila, G. Garrote, J.C. Parajó, Biofuels Bioprod. Biorefin. 6 (2012) 219–232.
[16] S.W. Fitzpatrick, ACS Symp. Ser. 921 (2006) 271–287.
[17] D.C. Elliott, J.G. Frye, Hydrogenated 5-Carbon Compound and Method of Making, US, 1999.
[18] S. Bayan, E. Beati, La Chim. L'Ind. 23 (1941) 432–434.
[19] H. Heeres, R. Handana, D. Chunai, C. Borromeus Rasrendra, B. Girisuta, H. Jan Heeres, Green Chem. 11 (2009) 1247–1255.
[20] L. Deng, Y. Zhao, J. Li, Y. Fu, B. Liao, Q.-X. Guo, ChemSusChem 3 (2010) 1172–1175.
[21] D.J. Braden, C.A. Henao, J. Heltzel, C.C. Maravelias, J.A. Dumesic, Green Chem. 13 (2011) 1755–1765.
[22] I.T. Horvath, H. Mehdi, V. Fabos, L. Boda, L.T. Mika, Green Chem. 10 (2008) 238–242.
[23] J.-P. Lange, R. Price, P.M. Ayoub, J. Louis, L. Petrus, L. Clarke, H. Gosselink, Angew. Chem. Int. Ed. 49 (2010) 4479–4483.
[24] J.Q. Bond, D.M. Alonso, D. Wang, R.M. West, J.A. Dumesic, Science 327 (2010) 1110–1114.
[25] D.W. Rackemann, W.O.S. Doherty, Biofuels Bioprod. Biorefin. 5 (2011) 198–214.
[26] R. Weingarten, J. Cho, R. Xing, W.C. Conner Jr., G.W. Huber, ChemSusChem 5 (2012) 1280–1290.
[27] K.R. Heimlich, A.N. Martin, J. Am. Pharm. Assoc. Sci. Ed. 49 (1960) 592–597.
[28] P.C. Smith, H.E. Grethlein, A.O. Converse, Sol. Energy 28 (1982) 41–48.
[29] H.E.v. Dam, A.P.G. Kieboom, H.v. Bekkum, Starch 38 (1986) 95–101.
[30] Q. Xiang, Y. Lee, R. Torget, Appl. Biochem. Biotechnol. 115 (2004) 1127–1138.
[31] M. Moliner, Y. Román-Leshkov, M.E. Davis, Proc. Natl. Acad. Sci. 107 (2010) 6164–6168.
[32] Y. Román-Leshkov, M. Moliner, J.A. Labinger, M.E. Davis, Angew. Chem. Int. Ed. 49 (2010) 8954–8957.
[33] E. Nikolla, Y. Román-Leshkov, M. Moliner, M.E. Davis, ACS Catal. 1 (2011) 408–410.
[34] Y.J. Pagán-Torres, T. Wang, J.M.R. Gallo, B.H. Shanks, J.A. Dumesic, ACS Catal. 2 (2012) 930–934.
[35] T. Wang, Y. Pagán-Torres, E. Combs, J. Dumesic, B. Shanks, Top. Catal. (2012) 1–6.
[36] K. Kato, T. Doihara, F. Sakai, N. Takahashi, Kenkyu Hokoku – Nippon Senbai Kosha Chuo Kenkyusho 108 (1966) 361–364.
[37] A. Ohnishi, K. Kato, E. Takagi, Polym. J. 7 (1975) 431–437.
[38] R. Krishna, M.R. Kallury, C. Ambidge, T.T. Tidwell, D.G.B. Boocock, F.A. Agblevor, D.J. Stewart, Carbohydr. Res. 158 (1986) 253–261.
[39] G.C.A. Luijkx, F.v. Rantwijk, H.v. Bekkum, Carbohydr. Res. 242 (1993) 131–139.
[40] R. Weingarten, G.A. Tompsett, W.C. Conner Jr., G.W. Huber, J. Catal. 279 (2011) 174–182.
[41] A.P. Dunlop, Ind. Eng. Chem. 40 (1948) 204–209.
[42] D.L. Williams, A.P. Dunlop, Ind. Eng. Chem. 40 (1948) 239–241.
[43] R. Weingarten, W.C. Conner Jr., G.W. Huber, Energy Environ. Sci. 5 (2012) 7559–7574.
[44] A. Clearfield, D.S. Thakur, J. Catal. 65 (1980) 185–194.
[45] A.L. Ginestra, P. Patrono, M.L. Berardelli, P. Galli, C. Ferragini, M.A. Massucci, J. Catal. 103 (1987) 346–356.
[46] R.A.W. Johnstone, J.-Y. Liu, D. Whittaker, J. Chem. Soc. Perkin Trans. 2 (6) (1998) 1287–1288.
[47] S.M. Patel, U.V. Chudasama, P.A. Ganeshpure, Green Chem. 3 (2001) 143–145.
[48] A. Clearfield, D.S. Thakur, Appl. Catal. 26 (1986) 1–26.
[49] A.L. Ginestra, P. Patrono, Mater. Chem. Phys. 17 (1987) 161–179.
[50] S.M. Patel, U.V. Chudasama, P.A. Ganeshpure, React. Kinet. Catal. Lett. 76 (2002) 317–325.
[51] Y. Kamiya, S. Sakata, Y. Yoshinaga, R. Ohnishi, T. Okuhara, Catal. Lett. 94 (2004) 45–47.
[52] J. Jimenez-Jimenez, J. Merida-Robles, E. Rodriguez-Castellon, A. Jimenez-Lopez, M. Lopez Granados, S. del Val, I. Melian Cabrera, J.L.G. Fierro, Catal. Today 99 (2005) 179–186.
[53] C. Srilakshmi, K. Ramesh, P. Nagaraju, N. Lingaiah, P.S.S. Prasad, Catal. Lett. 106 (2006) 115–122.
[54] K.N. Rao, A. Sridhar, A.F. Lee, S.J. Tavener, N.A. Young, K. Wilson, Green Chem. 8 (2006) 790–797.
[55] C. Carlini, M. Giuttari, A. Maria Raspolli Galletti, G. Sbrana, T. Armaroli, G. Busca, Appl. Catal. A 183 (1999) 295–302.
[56] T. Armaroli, G. Busca, C. Carlini, M. Giuttari, A.M. Raspolli Galletti, G. Sbrana, J. Mol. Catal. A: Chem. 151 (2000) 233–243.
[57] F. Benvenuti, C. Carlini, P. Patrono, A.M. Raspolli Galletti, G. Sbrana, M.A. Massucci, P. Galli, Appl. Catal. A 193 (2000) 147–153.
[58] C. Carlini, P. Patrono, A.M.R. Galletti, G. Sbrana, Appl. Catal. A 275 (2004) 111–118.
[59] M. Gu, D. Yu, H. Zhang, P. Sun, H. Huang, Catal. Lett. 133 (2009) 214–220.
[60] N. Li, G.A. Tompsett, G.W. Huber, ChemSusChem 3 (2010) 1154–1157.
[61] N. Li, G.A. Tompsett, T. Zhang, J. Shi, C.E. Wyman, G.W. Huber, Green Chem. 13 (2011) 91–101.
[62] F.S. Asghari, H. Yoshida, Carbohydr. Res. 341 (2006) 2379–2387.
[63] R.M. West, D.J. Braden, J.A. Dumesic, J. Catal. 262 (2009) 134–143.
[64] Y.J. Pagán-Torres, J.M.R. Gallo, D. Wang, H.N. Pham, J.A. Libera, C.L. Marshall, J.W. Elam, A.K. Datye, J.A. Dumesic, ACS Catal. 1 (2011) 1234–1245.
[65] T. Hattori, A. Ishiguro, Y. Murakami, J. Inorg. Nucl. Chem. 40 (1978) 1107–1111.
[66] A. Sinhamahapatra, N. Sutradhar, B. Roy, A. Tarafdar, H.C. Bajaj, A.B. Panda, Appl. Catal. A 385 (2010) 22–30.

[67] D. Spielbauer, G.A.H. Mekhemer, T. Riemer, M.I. Zaki, H. Knözinger, J. Phys. Chem. B 101 (1997) 4681–4688.
[68] O. Kresnawahjuesa, R.J. Gorte, D.d. Olivera, L.Y. Lau, Catal. Lett. 82 (2002) 155–160.
[69] J.G. Tittensor, R.J. Gorte, D.M. Chapman, J. Catal. 138 (1992) 714–720.
[70] R.J. Gorte, Catal. Lett. 62 (1999) 1–13.
[71] H.K. Mishra, K.M. Parida, Appl. Catal. A 224 (2002) 179–189.
[72] U. Ciesla, G. Stucky, F. Schiith, F.B.C.D.S.G., L. Bonneviot, S. Kaliaguine, Studies in Surface Science and Catalysis, Elsevier, pp. 527–534.
[73] R.R. Pinto, P. Borges, M.A.N.D.A. Lemos, F. Lemos, J.C. Védrine, E.G. Derouane, F.R. Ribeiro, Appl. Catal. A 284 (2005) 39–46.
[74] P. Batamack, C. Dorémieux-Morin, R. Vincent, J. Fraissard, Chem. Phys. Lett. 180 (1991) 545–550.
[75] P. Batamack, C. Dorémieux-Morin, R. Vincent, J. Fraissard, J. Phys. Chem. 97 (1993) 9779–9783.
[76] L. Heeribout, V. Semmer, P. Batamack, C. Dorémieux-Morin, R. Vincent, J. Fraissard, Studies in Surface Science and Catalysis, Elsevier, pp. 831–840.
[77] V. Semmer, P. Batamack, C. Dorémieux-Morin, R. Vincent, J. Fraissard, J. Catal. 161 (1996) 186–193.
[78] L. Heeribout, V. Semmer, P. Batamack, C. Dorémieux-Morin, J. Fraissard, Microporous Mesoporous Mater. 21 (1998) 565–570.
[79] V. Semmer-Herlédan, L. Heeribout, P. Batamack, C. Dorémieux-Morin, J. Fraissard, A. Gola, E. Benazzi, Microporous Mesoporous Mater. 34 (2000) 157–169.
[80] Y. Sun, P. Afanasiev, M. Vrinat, G. Coudurier, J. Mater. Chem. 10 (2000) 2320–2324.
[81] W. Liu, Z. Song, T. Ikegawa, H. Nishiguchi, T. Ishihara, Y. Takita, Mater. Lett. 58 (2004) 3328–3331.
[82] G.L. Zhao, Z.Y. Yuan, T.H. Chen, Mater. Res. Bull. 40 (2005) 1922–1928.
[83] J. Jiménez-Jiménez, P. Maireles-Torres, P. Olivera-Pastor, E. Rodríguez-Castellón, A. Jiménez-López, D.J. Jones, J. Rozière, Adv. Mater. 10 (1998) 812–815.
[84] K.-I. Segawa, Y. Kurusu, Y. Nakajima, M. Kinoshita, J. Catal. 94 (1985) 491–500.
[85] K.-I. Segawa, Y. Nakajima, S.-I. Nakata, S. Asaoka, H. Takahashi, J. Catal. 101 (1986) 81–89.
[86] Z.-Y. Yuan, T.-Z. Ren, A. Azioune, J.-J. Pireaux, B.-L. Su, Catal. Today 105 (2005) 647–654.
[87] A.M. Puziy, O.I. Poddubnaya, A.M. Ziatdinov, Appl. Surf. Sci. 252 (2006) 8036–8038.
[88] J.L. Colón, D.S. Thakur, C.-Y. Yang, A. Clearfield, C.R. Martin, J. Catal. 124 (1990) 148–159.
[89] M.S. Holm, Y.J. Pagan-Torres, S. Saravanamurugan, A. Riisager, J.A. Dumesic, E. Taarning, Green Chem. 14 (2012) 702–706.
[90] F. Chambon, F. Rataboul, C. Pinel, A. Cabiac, E. Guillon, N. Essayem, Appl. Catal. B 105 (2011) 171–181.
[91] M.S. Holm, S. Saravanamurugan, E. Taarning, Science 328 (2010) 602–605.
[92] T. Okuhara, Chem. Rev. 102 (2002) 3641–3666.
[93] A. Corma, H. Garcia, Chem. Rev. 103 (2003) 4307–4365.
[94] M.T. Tran, N.S. Gnep, G. Szabo, M. Guisnet, Appl. Catal. A 171 (1998) 207–217.
[95] G.E. Kellum, J.R. Hahn, Anal. Chem. 40 (1968) 952–956.
[96] D. Tichit, D. El Alami, F. Figueras, Appl. Catal. A 145 (1996) 195–210.
[97] G.K. Chuah, S. Jaenicke, S.A. Cheong, K.S. Chan, Appl. Catal. A 145 (1996) 267–284.
[98] G.D. Yadav, J.J. Nair, Microporous Mesoporous Mater. 33 (1999) 1–48.
[99] K.T. Jung, A.T. Bell, J. Mol. Catal. A: Chem. 163 (2000) 27–42.
[100] J. Griffith Edward, Phosphorus Chemistry, American Chemical Society, pp. 86–101.
[101] A.I. Ahmed, S.A. El-Hakam, S.E. Samra, A.A. El-Khouly, A.S. Khder, Colloids Surf., A 317 (2008) 62–70.